A novel heteroleptic Cu(II)-phenanthroline-UDCA complex as lipoxygenase inhibitor and ER-stress inducer on cancer cell lines

Sebastiano Masuri[1], Lukáš Moráň[2,3], Tereza Vesselá[2], Enzo Cadoni[1], Maria Grazia Cabiddu[1], Lukáš Pečinka[4], Viktorie Gabrielová[2], Francesca Meloni[1], Josef Havel[4,5], Petr Vaňhara[2,4], Tiziana Pivetta[*,1]

[1]Department of Chemical and Geological Sciences, University of Cagliari, Cittadella Universitaria, 09042, Monserrato, Cagliari, Italy.
[2]Department of Histology and Embryology, Faculty of Medicine, Masaryk University, 62500, Brno, Czech Republic.
[3]Research Centre for Applied Molecular Oncology, Masaryk Memorial Cancer Institute, 65653 Brno, Czech Republic.
[4]Department of Chemistry, Faculty of Science, Masaryk University, 62500, Brno, Czech Republic.
[5]International Clinical Research Center**,** St. Anne's University Hospital, 65691, Brno, Czech Republic.

Abstract

A new heteroleptic copper(II) compound named C0-UDCA was prepared by reaction of $[Cu(phen)_2(OH_2)](ClO_4)_2$ (C0) with the bile acid ursodeoxycholic acid (UDCA). The resulting compound was able to inhibit the lipoxygenase enzyme showing more efficacy than the precursors C0 and UDCA. Molecular docking simulations clarified the interactions with the enzyme as due to allosteric modulation. The new complex showed antitumoral effect on ovarian (SKOV-3) and pancreatic (PANC-1) cancer cells at the Endoplasmic Reticulum (ER) level by activating the Unfolded Protein Response (UPR). In particular, the chaperone BiP (HSPA5), the pro-apoptotic protein CHOP (DDIT3) and the transcription factor ATF6 were upregulated in the presence of C0-UDCA. The combination of Intact Cell MALDI-MS and statistical analysis have allowed us to discriminate between untreated and treated cells based on their mass spectrometry fingerprints.

Keyword: copper complex, SKOV-3, PANC-1, lipoxygenase, molecular docking, solution equilibria

Introduction

Bile acids are hydroxylated steroid acids biosynthesized from cholesterol and predominantly found in the bile of mammal and other vertebrates. They are classified as primary (i.e. cholic acid CA, chenodeoxycolic acid CDA), whose biosynthesis take place in liver cells, and secondary (i.e. deoxycholic acid DCA, ursodeoxycholic acid UDCA), that are obtained from the primary ones through biochemical processes performed by intestinal bacteria.[1] Bile acids are involved in cholesterol catabolism and emulsification of lipid in the intestinal tract. In addition these compounds work as endocrine mediators activating several receptors (e.g. nuclear farnesoid X receptor (FXR) and pregnane X receptor (PXR), the G-protein coupled receptor TGR5, etc) that are involved in pathways such as glucose and lipid metabolisms.[2] UDCA (**Figure 1A**) is currently approved for the treatment of primary biliary cirrhosis and other cholestatic disorders.[3,4] In addition, this compound have shown to possess modulable activity, cytoprotective or cytotoxic, according to the cell-

type.[5] Studies of UDCA in combination with conventional anticancer drugs have pointed out that some common side effects of the former ones are attenuated by the presence of UDCA.[6]

After the discovery of cisplatin's cytotoxic properties, several copper-based metallodrugs have been prepared and tested, with the aim of designing novel anticancer compounds having a better toxicological profile.[7–9] Previous studies carried out in our research group have shown that Cu(II) complexes such as $[Cu(phen)_2(H_2O)](ClO_4)_2$ (C0, **Figure 1B**), $[Cu(phen)_2(L)](ClO_4)_2$ (where L are imidazolidine-2-thione and some N-alkylated derivatives) and $[Cu(phen)_2(Salubrinal)](ClO_4)_2$ are able to induce massive cell death in ovarian cancer cells (A-2780, SKOV-3) by activating the pro-apoptotic branch of the Unfolded Protein Response (UPR).[10,11] UPR is a coordinating adaptive program that responds to accumulation of improperly folded proteins in the endoplasmic reticulum (ER), a condition known as ER stress. Initiation of UPR can lead to adaptation or apoptosis, especially in a condition of prolonged or severe ER stress.[12] UDCA and its taurine-conjugated derivative (taursodeoxycholic acid, TUDCA), have been extensively studied as ER stress modulators, and proved to exert their cytoprotective activity acting as chemical chaperones.[13,14] Previous studies of TUDCA in combination with the mixed Cu(II) phenanthroline complexes cited above, have evidenced how the cytotoxicity of these compounds might be modulated by the presence of TUDCA itself.[10,11]

Given these premises, and considering that UDCA comprises a carboxylic group that might interact with Cu(II), we prepared a new heteroleptic copper complex from C0 and UDCA, named C0-UDCA, with the intent to combine and/or exploit the biochemical activities of the two precursors (**Fig. 1C**).

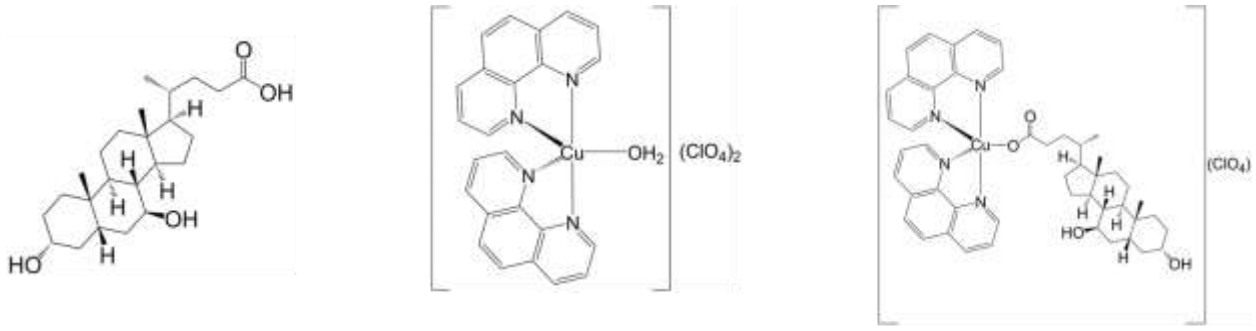

Fig. 1 Molecular structures and acronyms of the studied compounds.

The coordination mode, the solution equilibria, the antioxidant and anti-lipoxygenase activity of this novel compound were assessed by means of different experimental and theoretical studies. The anticancer activity of C0-UDCA against ovarian (SKOV-3) and pancreatic (PANC1) cancer cells was evaluated *in-vitro* and compared with the results obtained from its synthetic precursor C0. Based on previous studies when we showed the potentialities of intact cell mass spectrometry as a tool for cell quality control, bio-typing, and rapid identification of cell phenotype changes,[15,16] we verified whether we

would be able to discriminate between controls cancer cells treated with the studied compounds.

Results and Discussion

Synthesis and characterization of C0-UDCA

The reaction between the blue-green C0 and the colourless sodium salt of UDCA ($NaC_{24}H_{39}O_4$) led to the green complex $[Cu(phen)_2(C_{24}H_{39}O_4)](ClO_4)$ (C0-UDCA), whose stoichiometry has been established by elemental analysis (see experimental part) and mass spectrometry. In the ESI-MS spectrum of C0-UDCA (**Fig. 2**) a peak at 814 *m/z* was observed, due to the $[Cu(phen)_2(UDCA\text{-}H)]^+$ ion, obtained from the ionization of the neutral $[Cu(phen)_2(UDCA\text{-}H)](ClO_4)$ species. Other peaks, at 634, 457, 243 and 181 *m/z* due to the fragmentation of the molecular ion were observed depending on the experimental conditions. Precursor ion scan experiments showed that the fragments were originated in ESI-phase by the precursor $[Cu(phen)_2(UDCA\text{-}H)]^+$: *i*) the peak at 634 *m/z* was originated by loss of a phenanthroline unit to give the species $[Cu(phen)(UDCA\text{-}H)]^+$; ii) the peak at 243 *m/z* was originated by loss of the two phenanthroline units and the UDCA ligand, with the reduction of the metal ion, to give the species $[Cu(phen)]^+$ (the reduction of Cu(II) to Cu(I) is widely observed in ESI phase, depending on the used solvent)[17]; iii) finally, the peak at 181 *m/z* was due to the protonated phenanthroline species $[phen+H]^+$. The identity of the reported ions was confirmed by the fitting of the isotopic patterns (**Fig. S1**) and tandem mass experiments (see Mass spectrometry). High-resolution mass spectrum of C0-UDCA in the range 600-850 *m/z* was recorded to further confirm the composition of the peaks at 814 *m/z* and of its fragment at 634 *m/z* (**Fig. 3A**). As observable, the fitting of the isotopic pattern (**Fig. 3B**) and the matching between experimental and calculated exact masses (814.3532 u vs 814.3519 u and 634.2844 u vs 634.2832 u) confirmed the proposed stoichiometry.

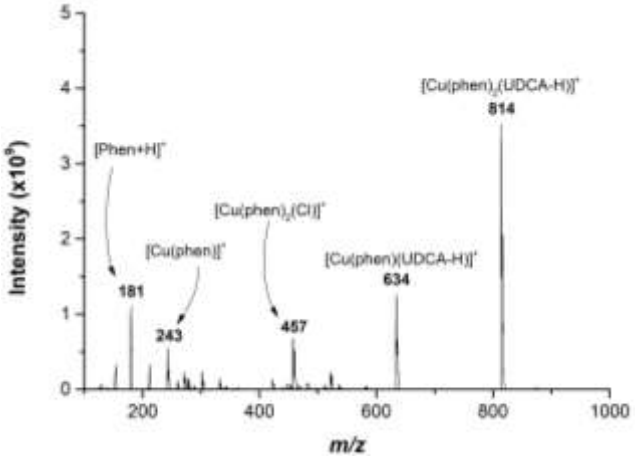

Fig. 2 ESI-MS spectrum of $[Cu(phen)_2(UDCA\text{-}H)](ClO_4)$ (methanol:water 1:1, 5000 volts at capillary). All the mass values are expressed as monoisotopic masses, computed as the sum of the masses of the primary isotope of each atom in the molecule (note that the monoisotopic mass may differ from the nominal molecular mass, especially for big molecules).

The novel copper complex $[Cu(phen)_2(UDCA\text{-}H)](ClO_4)$ proved to be stable in the solid state at room temperature, without precautions. It is not deliquescent. As regards its solubility, C0-UDCA is soluble in DMSO at 0.1 M concentration level, in CH_3CN at 0.01 M, in the H_2O:CH_3CN mixture (1:1) at 8 mM and in CH_3OH:H_2O at micromolar concentration. Solubility in water could be enhanced (up to 0.5 mM) by dissolving C0-UDCA in a minimal amount of DMSO at 40 °C prior to water addition. In this case, sonication or vigorous mixing should be avoided to prevent the formation of emulsions.

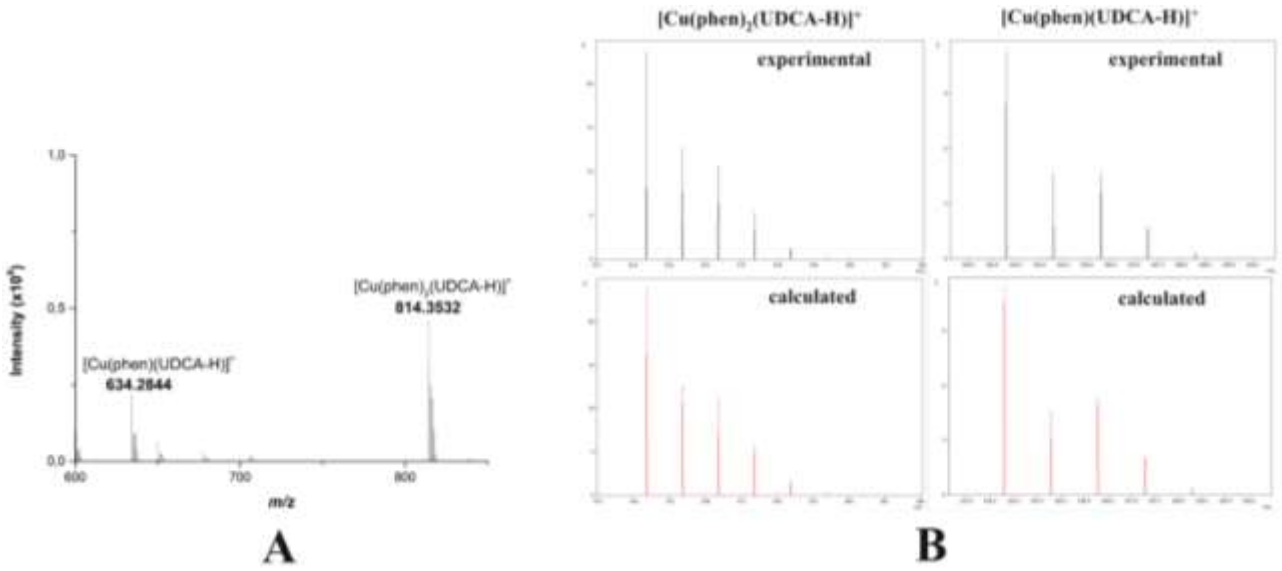

Fig. 3 (**A**) High-resolution mass spectrum of **C0-UDCA** in the 600-850 *m/z* range, (**B**) experimental and calculated isotopic pattern for peaks at 814 and 634 *m/z*, (methanol:water 1:1). All the mass values are expressed as monoisotopic masses.

Stock solutions of C0-UDCA in DMSO or CH_3CN are stable at 4 °C up to 6 months, while stock solutions in H_2O:CH_3CN mixture (1:1) could be stored at 25 °C for 2 weeks. The stability of C0-UDCA in phosphate buffer was assessed by following the spectral variation in the 200–325 nm range for 24 hrs recording 1 spectrum every 60 minutes (**Fig. S2**). No significant variations in the shape and intensity of the spectra were observed.

Complex formation constant of C0-UDCA

The complex formation constant was studied in 0.05M phosphate buffer at pH 7.4. At this pH UDCA is present as monoanionic species due to the proton loss from the carboxylic moiety. The method of continuous variation (Job's method) was applied to determine the number of the formed complexes and the related stoichiometry.[18,19] Absorption spectra collected varying the reactants molar fractions are reported in **Fig. S3A**, while the absorbance at 271 nm, corrected for the absorption of pure species, are reported as a function of the ligand molar fraction in **Fig. S3B**. These data clearly show the formation of a 1:1 ligand to metal complex (χ_L = 0.49).

Once established the formation of a unique 1:1 ligand to metal complex, the related formation constant was determined by spectrophotometric titrations. Selected spectra recorded during the titration of **C0** with deprotonated UDCA are reported in **Fig. 4**, corrected for the dilution. As observable, the addition of the ligand resulted in a slight increment of the absorbance at 271 nm, until the ligand/metal molar ratio reached the unity value (see inset in Fig. 4A). The Factor Analysis of the spectrophotometric data indicated three linearly independent absorbing species in solution, i.e. the two reactants and the formed complex. The complex formation constant, expressed as log β, was calculated as 5.2 ± 0.2 M^{-1}. The pure spectra of the reactants and the formed complex are reported in **Fig. 4.** The absorption bands of C0 and C0-UDCA fall in the same region, however the mixed complex shows absorptivity value higher at 271 nm.

Coordination mode in C0-UDCA

Since any attempt to obtain single crystals suitable for X-ray analysis was unsuccessful, the coordination mode for the novel C0-UDCA complex was proposed by combining the experimental data (UV-Vis, IR spectroscopy, ESI-

MS and tandem MS spectrometry) with the theoretical calculations.

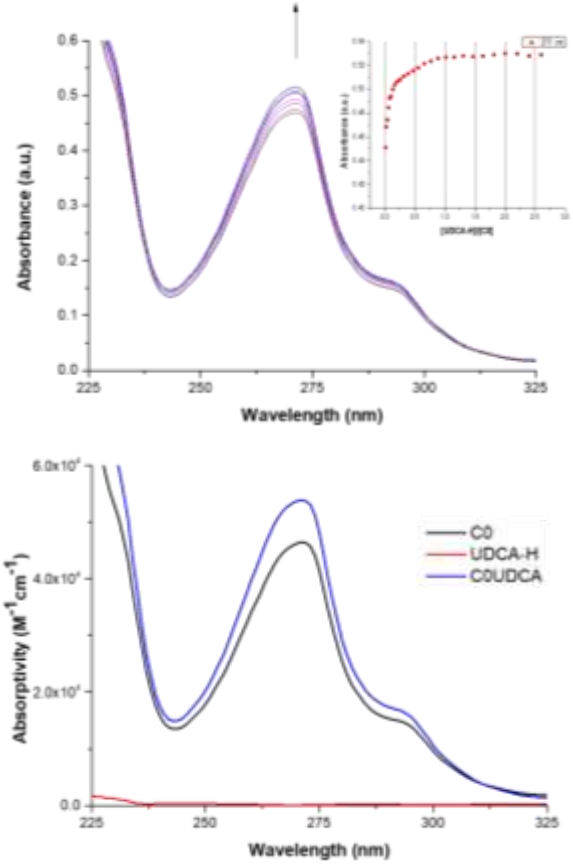

Fig. 4 Selected spectra collected during the titration of (upper) 2.12×10^{-5} mmol of **C0** with UDCA-H (2.55×10^{-5} M) in 225-325 nm range, corrected for the dilution; (bottom) absorptivity spectra of **C0**, UDCA-H and C0-UDCA (phosphate buffer 0.05 M, pH 7.4, 25 °C, 1 cm optical path length).

UV-Vis. The absorption spectrum of C0-UDCA in CH_3CN solution in the region 450 - 1100 nm is reported in **Fig. S4** and features a maximum at 686 nm and a shoulder at 942 nm. In analogy with the absorption spectra of variously ternary Cu(II) bis-phenanthroline complexes previously characterized,[20] a penta-coordinated geometry might be proposed also for the novel complex C0-UDCA.

FT-IR. FT-IR spectrum of C0-UDCA (**Fig. S5C**) shows a large and intense band at 3410 cm^{-1}, that can be ascribed to the hydroxyl groups of the UDCA moiety, while the two peaks at 2933 and 2865 cm^{-1} are relative to the -CH- stretching frequencies. Asymmetric and symmetric stretching peaks of oxygen carboxylate group ($\upsilon_{asym}(OCO)$ and $\upsilon_{sym}(OCO)$) fall at 1565 and 1375 cm^{-1} respectively. In the FT-IR spectrum of sodium ursodeoxycholate (**Fig. S5A**) the same bands appear at 1561 and 1406 cm^{-1} respectively. The parameter $\Delta(OCO) = \upsilon_{asym}(OCO) - \upsilon_{sym}(OCO)$ is commonly used to gain more insights regarding the coordination mode of carboxylate functional groups in metal complexes. In particular, a $\Delta(OCO)complex > \Delta(OCO)ligand$ is indicative of an unidentate coordination mode of the carboxylic group.[21,22] Considering that $\Delta(OCO)$ for C0-UDCA equals to 190 cm^{-1}, which is higher than the same value for sodium ursodeoxycholate (155 cm^{-1}), we can assume that also for C0-UDCA coordination of carboxylate group to the metal centre takes place in mono-dentate fashion. Signals of the phen moieties are visible at 3068, 1519, 1430, 1386, 851, 724, 624 cm^{-1} (see for comparison IR spectrum of the precursor C0, **Fig. S5B**), while the wide band in the region 1150-1030 is due to the perchlorate anion.

Mass spectrometry. Tandem MS experiments at different collision energies (CE) were performed to identify the nature of the peaks containing Copper (II), phenanthroline and UDCA and give more insights about the structure of the novel C0-UDCA complex. As regards the ion $[Cu(phen)_2(UDCA\text{-}H)]^+$ (*m/z* 814), the formation of a product ion at *m/z* 634 is evidenced from CE 5V (**Fig. 5**). The former ion, whose formula was previously proposed as $[Cu(phen)(UDCA\text{-}H)]^+$, is originated from precursor at *m/z* 814 by loss of one phenanthroline unit (**Fig. S6A**). As observed in **Fig. 5**, a gradual decrease in intensity for the peak at *m/z* 634 is observed, as CE is increased. This feature is consistent with further fragmentation processes of the former ion. In particular, from CE 35V, two peaks at *m/z* 260 ($[Cu(phen)(OH)]^+$) and 243 ($[Cu(phen)]^+$) were

observed. The first product ion might come from its precursor by the rearrangement showed in **Fig. S6B**, i.e. transposition of a Hα from UDCA moiety and subsequent closure of a Cα=Ccarbonyl double bond with loss of a neutral ketene. The second fragment is originated by the radical process depicted in **Fig. S6C**, which brings to a Cu(I) ion with the loss of the UDCA moiety as a radical. CID experiments performed on the ion at *m/z* 634 (**Fig. S7**) showed the same pattern, thus confirming the fragmentation scheme previously reported. The breakdown curves, obtained reporting the peak intensity *vs* CE, show the relative stability of the formed species: i) at 0 CE the unique stable species is $[Cu(phen)_2(UDCA\text{-}H)]^+$; ii) it is necessary to apply 20 volt as CE to completely convert $[Cu(phen)_2(UDCA\text{-}H)]^+$ in $[Cu(phen)(UDCA\text{-}H)]^+$; iii) at CE higher than 30 volts $[Cu(phen)(UDCA\text{-}H)]^+$ is fragmented with loss of the UDCA ligand.

DFT calculations. Geometry optimization for both UDCA-H and Cu(II) complex $[Cu(phen)_2(UDCA\text{-}H)]^+$ were performed using the same computational setup employed for the parent copper complex $[Cu(phen)_2(H_2O)]^+$ and other similar Cu(II) complexes, as previously reported.[11]

In particular, assessment of the DFT performance for $[Cu(phen)_2(H_2O)]^+$ (whose coordinates were taken starting from **C0** single X-Ray structural data) revealed a very good agreement between experimental and calculated data. In **Fig. S8A** DFT optimized geometry for UDCA-H ligand is reported. As observable from frontier molecular orbital analysis (**Fig. S8B**), HOMO and HOMO-1 molecular orbitals are highly centred on oxygen carboxylate moiety, thus supporting a coordination from this functional group. Selected bonds, angles and dihedrals are reported in **Table S1**.

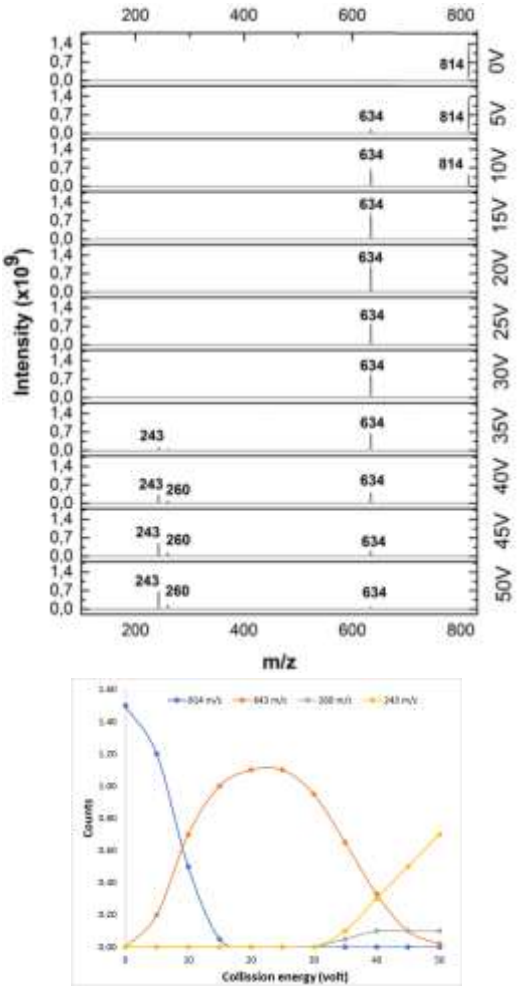

Fig. 5 Tandem MS fragmentations and breakdown curves at different collision energy (0 - 50 volts).

Geometry optimization at DFT level for $[Cu(phen)_2(UDCA\text{-}H)]^+$ reveals a geometry closer to a square pyramidal than to a trigonal bipyramidal, as suggested by the value of geometrical parameter $\tau = \frac{\beta-\alpha}{60°}$ of 0.22.[23] The former distortion is also evident at bond lengths level, where elongation of Cu-N2 (2.309 Å) is accompanied by shortening of Cu-N3, Cu-N1 and Cu-O1 bonds (2.040, 2.059 and 1.958 Å respectively). These results are in agreement with several mono and binuclear Cu(II) bis-phenanthroline complexes coordinated by carboxylate functional groups.[24–27] Selected bonds, angles and dihedrals are reported in **Table S2**. Atomic charges, computed at NPA level (**Table S3**), show on copper ion a significant lower

atomic charge (1.39) compared with its formal charge +2, while on N1-4 and O1 atoms high negative calculated charges were evidenced. This trend suggests a partial charge transfer to the metal centre from the coordinating atoms of ligands, as evidenced at frontier Molecular Orbital level, where both α and β SOMOs are centred on UDCA moiety, while α and β LUMOs are redistributed among the metal centre and one of the phenanthroline ligands (**Fig. 6**).

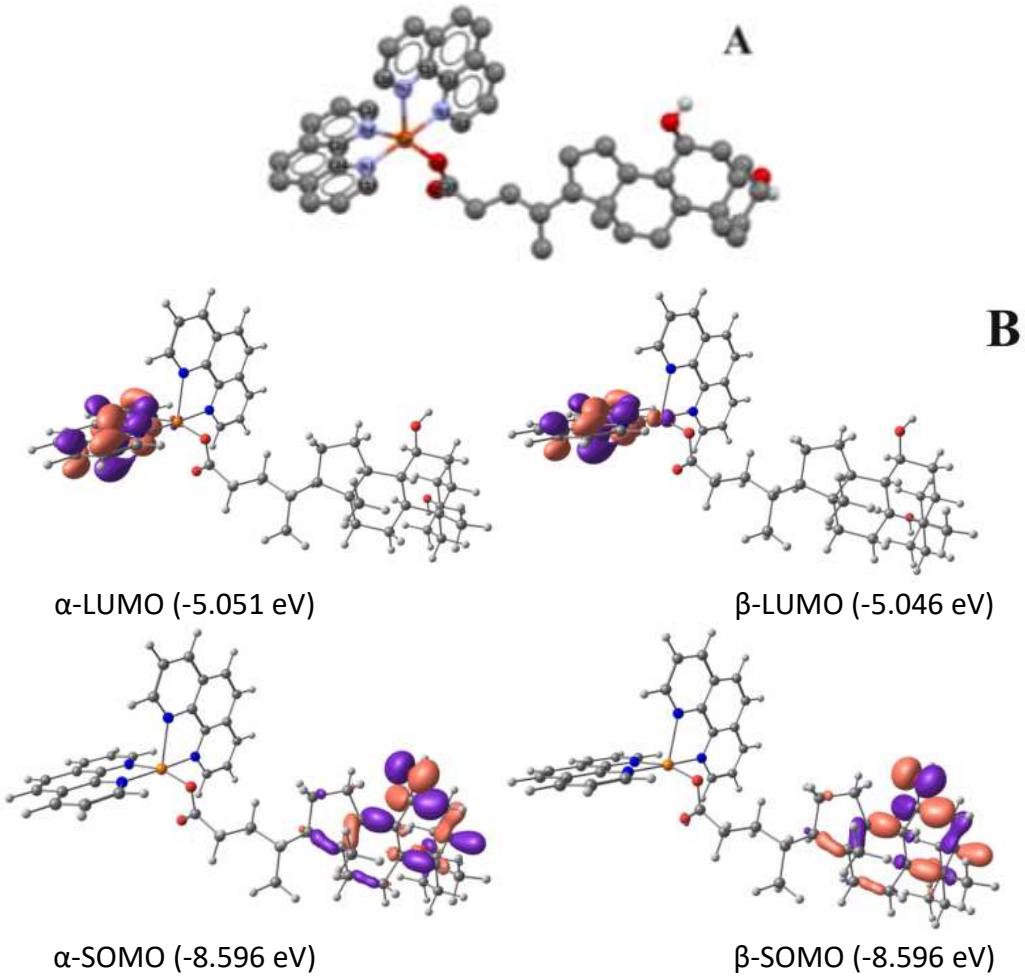

Fig. 6. Molecular drawings and atom labelling schemes for $[Cu(phen)_2(UDCA\text{-}H)]^+$ (**A**) at the DFT-optimized geometry. Isosurface drawings of selected frontier molecular orbitals calculated (**B**) for $[Cu(phen)_2(UDCA\text{-}H)]^+$ (contour value: 0.05). Non-polar hydrogen atoms in (**A**) are omitted for clarity.

Soybean lipoxygenase inhibition: Experimental study

Lipoxygenases constitute a widespread group of Iron dioxygenases that are involved in the production of leukotrienes through the arachidonic cascade pathway.[28] Increased levels of human lipoxygenases, such as 5-LOX have been observed in several types of cancers, and some 5-LOX inhibitors have shown the ability to arrest the tumour cell proliferation and induce apoptosis.[29] For this reason, we studied the inhibition of the UDCA and C0-UDCA towards these enzymes using Soybean Lipoxygenase as the model. The experiments were performed keeping constant the concentration of substrate and enzyme and varying that of UDCA, or C0-UDCA. The results obtained were compared with the ones obtained for C0.[11] In the absence of an inhibitor, the enzyme requires about 90 minutes to convert the linoleate substrate to 13-hydroperoxylinoleic. In the presence of **UDCA**,

the substrate conversion is reduced till the 80 % but it is required a concentration of 600 microM (**Fig. 7A** and **S9A**). In the presence of C0-UDCA, the inhibition appears more potent, being almost complete at approx. 9 microM (**Fig. 7B** and **S9B**).

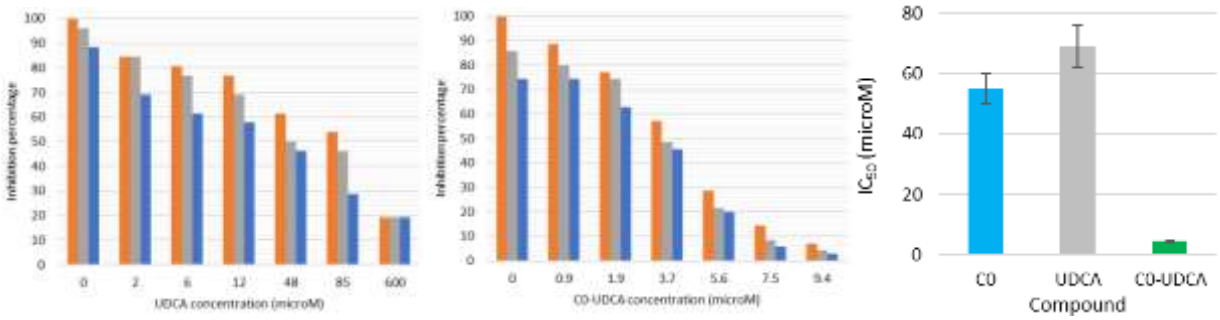

A **B** **C**

Fig 7. Lipoxygenase inhibition percentage of UDCA (**A**) and C0-UDCA (**B**) at different concentrations, after 90, 50 and 35 minutes (orange, grey and blue columns, respectively; mean of three independent measure, standard deviation was ≤ 0.6 %). Note that the X-scales are different for the two molecules. Calculated IC50 for C0, UDCA and C0-UDCA (**C**).

The inhibition percentage (**IP**) varies with the time for every given concentration (**Fig. S10**), becoming invariant after 50 min for **UDCA** and 35 min for **C0-UDCA**. These two values were chosen as the time reference to calculate the IC_{50} value, i.e., the concentration required to inhibit 50% of enzyme activity. For the two compounds, IC_{50} resulted to be 69 ± 7 µM for UDCA and 4.4 ± 0.1 µM for C0-UDCA (**Fig. 7C**). Since the IC_{50} of C0 is for the same substrate and enzyme 55 ± 5 µM,[11] the inhibition activity of C0-UDCA results to be 12.5 and 17 higher than that of C0 and UDCA, respectively. These results suggest that the insertion of the UDCA auxiliary ligand in the $[Cu(phen)_2]$ core affects positively the inhibitory ability towards lipoxygenase. Moreover, the different trends shown in Fig. S10 for UDCA and C0-UDCA suggest possible different mechanisms involved in the reaction with the enzyme. A similar behaviour was observed for C0 and the mixed complex $[Cu(phen)_2(Salubrinal)](ClO_4)_2$.[11]

Soybean lipoxygenase inhibition: Theoretical study

Since C0-UDCA was able to interact with Soybean Lipoxygenase, a theoretical study aiming to describe the kind of interaction was performed by Molecular Docking (MD). MD calculations were performed for UDCA-H and $[Cu(phen)_2(UDCA\text{-}H)]^+$ using the structure of Soybean Lipoxygenase (PDB:1N8Q) as receptor model. Both compounds were initially docked using a grid box centred on the Iron cofactor considering the ability of various molecules at inhibiting Soybean Lipoxygenase by targeting their catalytic binding site. Results obtained for both UDCA-H and $[Cu(phen)_2(UDCA\text{-}H)]^+$ show high positive docking score values (13.42 kcal/mol and 75.96 kcal/mol respectively) that could be attributed to the hindering shape effects derived to the bulky nature of the ligands. For this reason, docking calculations on the former compounds were repeated using a grid box located between the C-terminus and N-terminus domains of Soybean Lipoxygenase. In this case, docking score values of -7.80 and -9.39 kcal/mol were obtained for Ursodeoxycholate and $[Cu(phen)_2(UDCA\text{-}H)]^+$ respectively (**Fig. S11**). Analysis of the docked pose of UDCA-H (**Fig. 8**) indicates hydrogen bonds with Cys145 and His548 and alkyl interactions with the Val539 residue. In the case of $[Cu(phen)_2(UDCA\text{-}H)]^+$, a closer inspection of the molecular interactions (**Fig. 9**) reveals mainly hydrogen bond

interactions with Gly265 and Gln96, carbon-hydrogen bond with Gly93 and Asn788, and π-alkyl interactions with Phe126. The conformation adopted by the highest-docking score of $[Cu(phen)_2(UDCA\text{-}H)]^+$ is stabilized by intramolecular π-sigma interactions between the ursodexoycholate moiety and one of the phenanthroline units.

These findings suggest for the studied compounds a potential allosteric inhibition mode, that might take place, for instance, by reducing the enzyme affinity for the substrate.

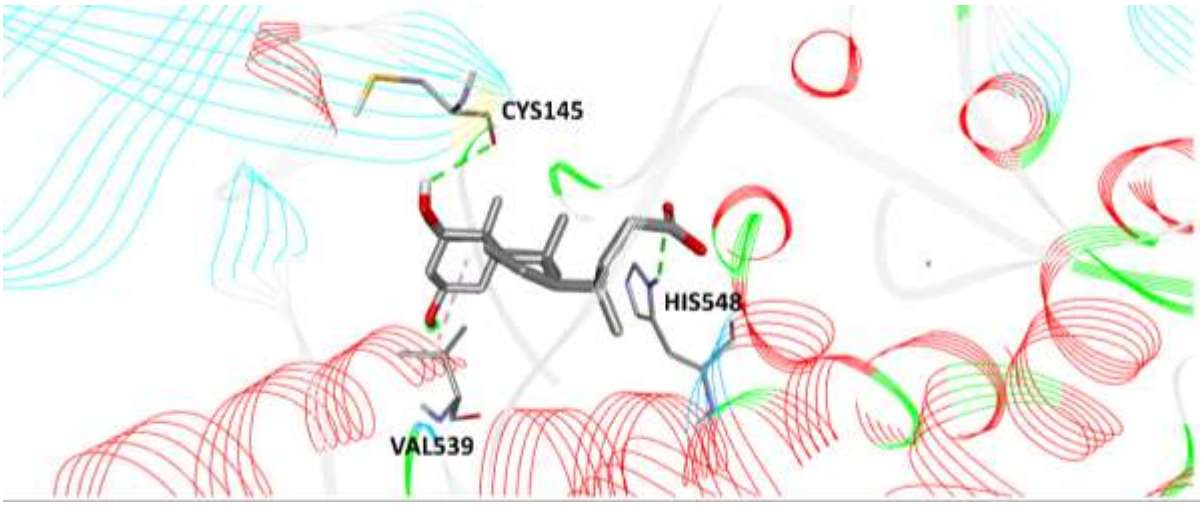

--- hydrogen bond; --- alkyl interaction

Fig. 8 Docked poses of UDCA-H and intermolecular interactions with the surrounding residues of soybean lipoxygenase.

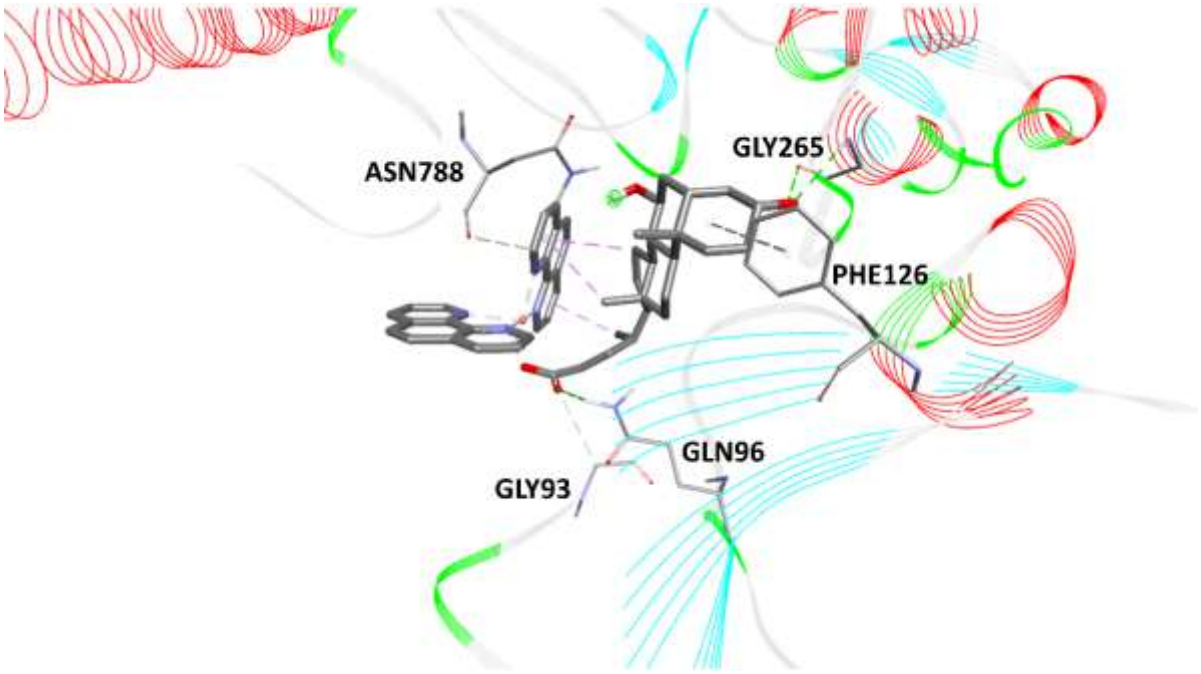

--- hydrogen bond --- π-alkyl --- C-hydrogen bond donor --- π-sigma

Fig. 9 Docked poses of $[Cu(phen)_2(UDCA\text{-}H)]^+$ and intermolecular interactions with the surrounding residues of soybean lipoxygenase.

Cell proliferation study

The antiproliferative activity of C0-UDCA and of its precursor C0 was evaluated on ovarian (SKOV-3) and pancreatic (PANC-1) cancer cells. The IC_{50} values of the studied compounds were determined from MTT results (**Table 1**).

Table 1. Anticancer activity of the studied compounds reported as IC_{50} values (concentration of drug able to induce cell death by 50%).

Compound	IC_{50} (μM)	
	SKOV-3	PANC-1
C0	7.9(1)	13.0(1)
C0-UDCA	6.8(1)	7.0(1)

As can be seen, on SKOV-3 cells the biological activity of C0-UDCA and C0 are comparable, while in the case of PANC-1 C0-UDCA shows a double antiproliferative activity with respect of C0. The metabolic assay, documenting mitochondrial performance by the MTT assay is reported in **Fig. S12**. To study the effect on the cell proliferation, the SKOV-3 and PANC-1 cancer cells were treated with C0-UDCA, C0, TUDCA or left untreated, and the cell number was determined after 48 hrs (**Fig. 10**).

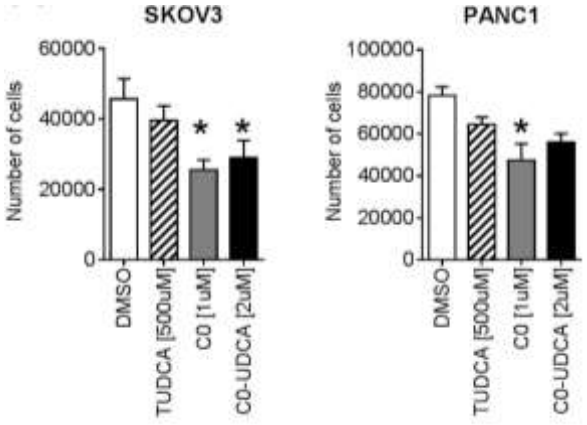

Fig. 10. The cell numbers of SKOV-3 and PANC-1 cells after 48 hrs culture in presence of C0, TUDCA and C0-UDCA. The starting number of cells was 20 000. Plot shows means and SDs from three independent experiments.

C0 and C0-UDCA decreased the proliferation rate of both the kind of cells, then, to understand the possible mechanism causing the drop in the cell numbers, we stained the intact cells with FITC-conjugated Annexin V (AV) and propidium iodide (PI). Since AV interacts with the externalized phosphatidylserine of the plasma membrane, while propidium iodide interacts with the DNA, the dual staining helps to discriminate between apoptotic and necrotic cell death. In fact, Annexin V-positive and PI-negative staining indicate apoptosis while Annexin V-positive and PI-positive indicate necrosis. Results are shown in **Fig. 11**.

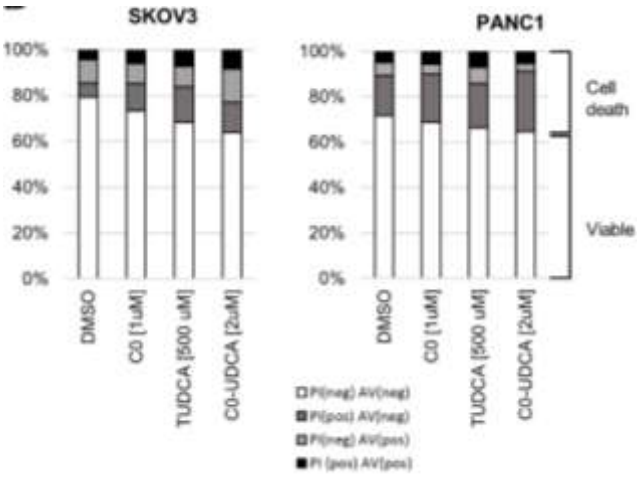

Fig. 11 C0-UDCA increases externalization of phosphatidylserine in SKOV-3 cells. The cells were cultured as described in Fig. 9, then the exposure of phosphatidylserine on the cell surface was assessed by FACS using FITC-conjugated Annexin V probe. Cell viability was measured by propidium iodide staining. Typical results of three independent experiments are shown.

Both C0-UDCA and C0 induced significant cell death as indicated by a decrease of viable cells (white zone in Fig. 10).

In the SKOV-3 cells, C0-UDCA preferentially induced the programmed cell death as indicated by increase in Annexin V positive, propidium iodide negative cell (early stage apoptotic 40%, late stage apoptotic 23%, necrotic 37%) while the

precursor C0 appears to act in the opposite way (necrotic 44%, early stage apoptotic 30% and late stage apoptotic 26%), as also TUDCA (necrotic 48%, early stage apoptotic 27% and late stage apoptotic 25%). In PANC-1 cells, the propidium iodide positive cells prevailed of over double positive cells, indicating secondary necrosis for both C0-UDCA (necrotic 74%, late stage apoptotic 18% and early stage apoptotic 8%) and C0 (necrotic 67%, late stage apoptotic 21% and early stage apoptotic 12%). Also TUDCA acts in same way (necrotic 58%, late stage apoptotic 23% and early stage apoptotic 19%).

Antitumoral action mechanism

To reveal the effects of C0-UDCA and its precursor at the level of protein synthesis, we performed a western blotting (**Fig. 12, Fig. S13**) and immunofluorescence staining (**Fig. 14**) on SKOV-3 and PANC1 cell lines. The chemical chaperone TUDCA did not affect the levels of ER stress associated proteins in any of the cases.

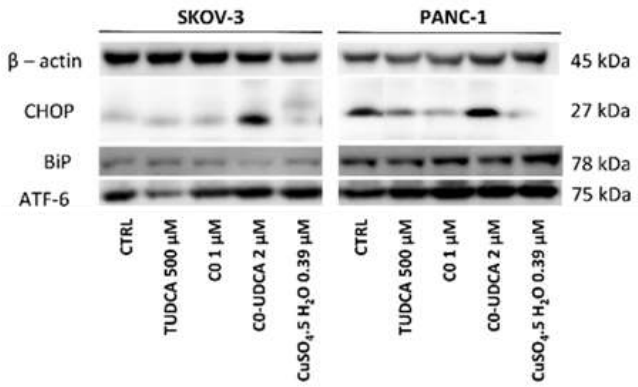

Fig. 12. Protein expression of BiP, CHOP and ATF6 in SKOV-3 and PANC-1 cells treated for 24 hrs with **C0-UDCA** at 2.0 µM. β-Actin was used as a control of equal loading.

On the other hand, the presence of C0 and C0-UDCA indicated the upregulation of the chaperone BiP (HSPA5) and the pro-apoptotic protein CHOP (DDIT3). The activation of ER stress is also visible on the levels of the transcription factor ATF6 which levels increased especially after exposure to C0.

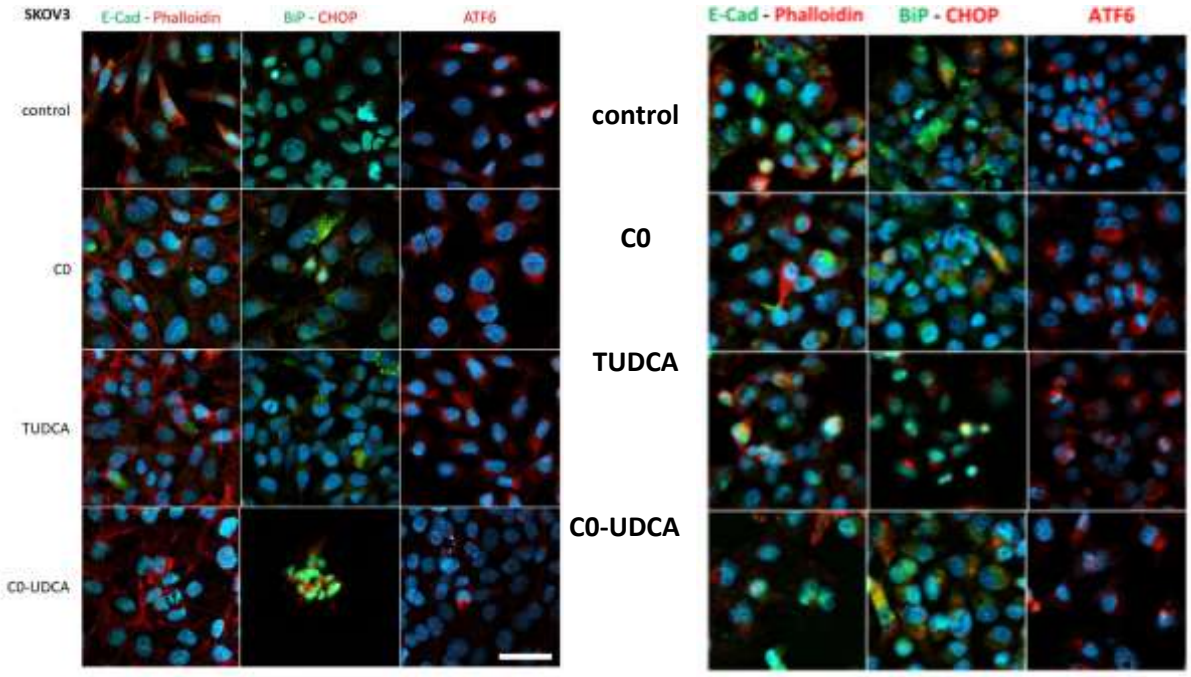

Fig. 13. Protein levels of ER stress associated markers BiP, CHOP and ATF6. In SKOV-3 and PANC-1 cells treated for 24 hours with C0, TUDCA and C0-UDCA as documented by immunofluorescence. Phalloidin was used for cytoskeleton filaments staining. Nuclei (blue) are visualized by Hoechst staining. The scale bars indicate 10 µm.

Cellular fingerprints

Recently we have introduced a methodology of intact cell mass spectrometry as a tool for cell quality control, bio-typing, and cell phenotype changes rapid identification.[15,16] Here we were also able to detect changes in the biological background of treated cells, after measuring the characteristic spectral fingerprints of individual samples. The peaks with the largest differences were selected (**Fig. 14**) and a PCA statistical analysis was performed (**Fig. 15**), thanks to which we were able to distinguish control cells and cells treated with C0, TUDCA and C0-UDCA, indicating different effects of C0-UDCA on SKOV3 cells than C0 or TUDCA alone.

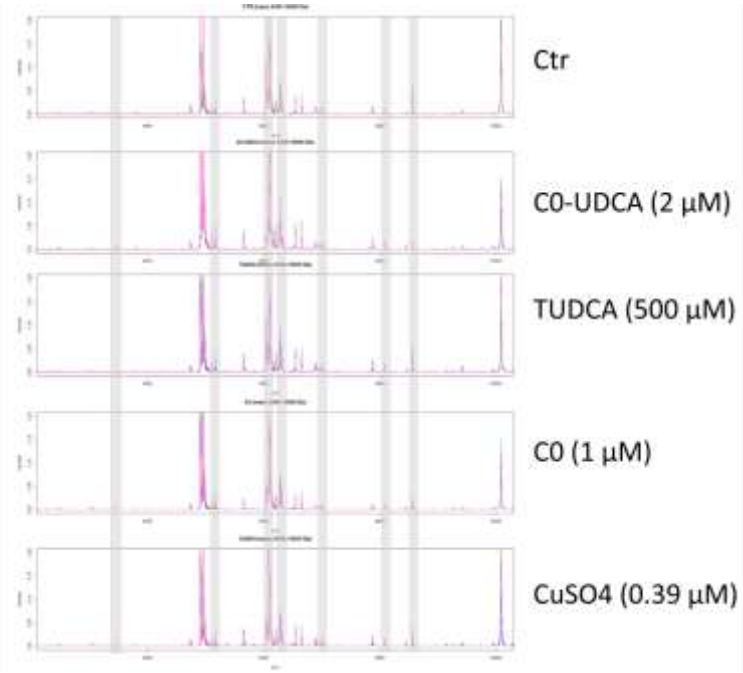

Fig. 14 Mass spectra of selected *m/z* regions of treated cells with the main differences in individual spectra highlighted.

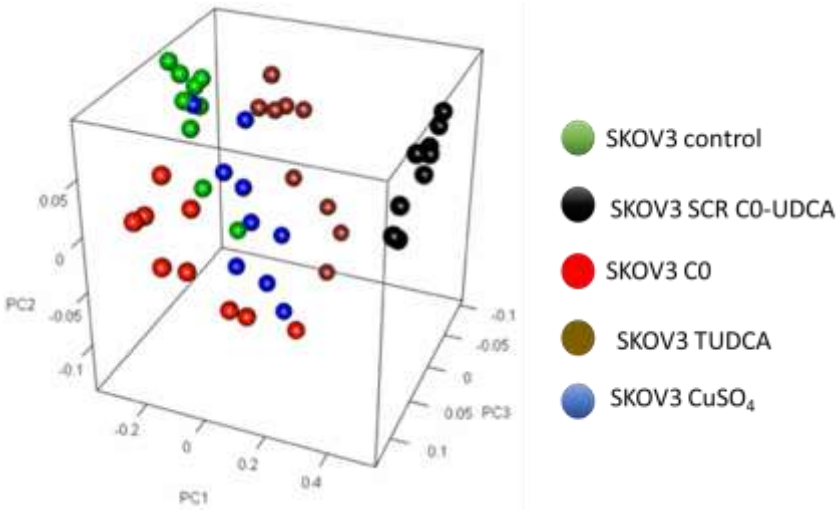

Fig. 15 PCA statistical analysis, individual treatments cluster into specific groups.

Conclusions

This study shows how the chemical interaction between the $[Cu(phen)_2(H_2O)]^{2+}$ complex and the bile acid UDCA leads to the formation of the novel heteroleptic complex C0-UDCA.

Studies with lipoxygenase evidenced how the complex $[Cu(phen)_2(UDCA\text{-}H)]^{+}$ presents a anti lipoxygenase activity higher than the precursors UDCA (17x) and C0 (12.5x), showing a decrease of the concentration required to inhibit half the enzyme, from 55 µM of the sole C0 or 69 of the sole UDCA, to 4.4 µM of C0-UDCA. Molecular Docking studies indicate for C0-UDCA a potential allosteric mechanism. Since leukotrienes, derived from the 5-lipoxygenase pathway, are mediators of inflammation and allergy and are also involved in cardiovascular diseases, cancer and osteoporosis, the availability of molecules able to interact with 5-LOX is a challenge in the development of therapeutics, and in this field our results find an interesting scene.

Furthermore, C0-UDCA can inhibit the cell growth and reduces cell viability of both ovarian (SKOV-3) and pancreatic (PANC-1) cancer cells at micromolar level. Mechanistic studies, performed on both cell lines, indicate that this compound exerts its anticancer properties by activating the UPR pathway. In particular, in the presence of C0-UDCA the chaperone BiP (HSPA5) and the pro-apoptotic protein CHOP (DDIT3) are upregulated. The activation of ER stress is also visible on the levels of the transcription factor ATF6 which levels increased especially after exposure to C0.

The combination of IC-MALDI-MS and statistical analysis allowed us to distinguish between controls and cells treated with the C0, C0-UDCA and TUDCA compounds.

All these results, achieved thanks to the interdisciplinary approach proposed in this study, might provide new hints for the design and synthesis of novel bioactive Cu(II) coordination compounds.

Methods

Reagents

Acetonitrile, isopropanol, absolute ethanol, sodium linoleate, lipoxygenase, tris(hydroxymethyl)aminomethane hydrochloride (TRIS), dimethyl sulfoxide (DMSO) were purchased from Merck (Milan, Italy). Basic copper carbonate and ursodeoxycholic acid were purchased from Alfa-Aesar (Kandel, Germany). 3-(4,5-dimethylthiazol-2-yl)-2,5-diphenyltetrazolium bromide (MTT) was purchased from Sigma-Aldrich (Prague, Czech Republic). The commercial reagents were used as received, without any further purification. Ultrapure water was obtained with a MilliQ Millipore apparatus (Milan, Italy).

Mass spectrometry studies

Low resolution mass spectra were recorded using a triple quadrupole (QqQ) Varian 310-MS (Palo Alto, CA, USA) using the atmospheric-pressure ESI technique. Each the sample solution was infused into the ESI source using a programmable syringe pump (1.25 mL/h constant flow rate). A dwell time of 14 s was used and the spectra were accumulated for at least 10 min to increase the signal-to-noise ratio, as previously adopted for metal complexes [30]. Mass spectra were recorded in the *m/z* 100 – 1000 range. The experimental conditions were: needle voltage 3500 V, shield 800 V, source temperature 60 °C, drying gas pressure 20 psi, nebulizing gas pressure 20 psi, detector voltage 1450 V. Tandem MS experiments were performed using argon as the collision gas (1.8 psi). The collision energy was varied from 5 to 50 V. High resolution mass spectra were recorded on a Thermofisher ESI-MS/MS-ORBITRAP-ELITE and Velos PRO (Waltham, MA, USA). Sample solutions were infused directly into the ESI source using a

programmable syringe pump at a flow rate of 5 µL/min. Mass spectra were recorded in the *m/z* 600 – 850 range. The experimental conditions were needle voltage 2.5 kV, shield 0.8 kV, source temperature 50 °C, drying gas pressure 20 psi, nebulizing gas pressure 20 psi, detector voltage 1.3 kV. The isotopic patterns of the measured peaks in the mass spectra were analysed using the mMass 5.5.0 software package.[31,32] All the mass values are indicated as monoisotopic masses, computed as the sum of the masses of the primary isotope of each atom in the molecule (note that the monoisotopic mass may differ from the nominal molecular mass, especially for molecules having high molecular weight).

Spectroscopic studies

UV–Visible spectrophotometric measurements were performed with an Agilent Cary 60 spectrophotometer (Palo Alto, CA, USA) using a 1 cm quartz cell. UV-Vis spectra were acquired at 25 °C in the 200 – 1100 nm range. Solution equilibria between C0 and UDCA were evaluated by means of spectrophotometric titrations performed in phosphate buffer (0.05 M, pH 7.4). The number of linearly independent absorbing species was obtained by applying eigenvalues analysis on the absorbance data matrix. The complex formation constant, expressed as overall association constant, was calculated using the Hyperquad 2006 program.[33] The stoichiometry of the formed complex was also evaluated using the continue variation method (Job's plot).[19,34] IR spectra were acquired with a Bruker Vector 22 spectrophotometer (Ettlingen, Germany), preparing the samples as KBr pellets.

Synthesis

C0. The precursor $[Cu(phen)_2(OH_2)](ClO_4)_2$ (C0) was prepared as previously described.[20] In brief, perchloric acid was added to an ethanolic suspension of $Cu_2(CO_3)(OH)_2$. The resulting blue solution was cooled and an ethanolic solution of 1,10-phenanthroline, at 1:2 metal:ligand molar ratio, was slowly added, observing the formation of a blue-green precipitate. This solid was filtered, washed with ethanol and dried at room temperature (Yield 85 %).

Sodium Ursodeoxycholate (prepared for FT-IR measurements). UDCA (0.2318 mmol) was suspended in acetonitrile (5.0 mL), then 1 eq of NaOH 1.0 M water solution (232 µL) was added to the suspension. The reaction mixture was left under stirring at r.t. for 1hr. The product was recovered by filtration, washed with acetonitrile, and dried. 0.0411 g (Yield 43%). Elemental analysis % for $C_{24}H_{39}NaO_4$ was expected C 69.53, H 9.48, found C 69.55, H 9.52. FT-IR (KBr), cm^{-1}:1561 $\upsilon_{asym}(OCO)$, 1406 $\upsilon_{sym}(OCO)$.

C0-UDCA. $[Cu(phen)_2(UDCA\text{-}H)](ClO_4)$ was prepared as following: UDCA (0.2385 mmol) was treated with 1 eq of NaOH to obtain the corresponding sodium salt. This solution was slowly added to a water suspension of C0 (1 eq, 10 mL). The progressive formation of a pale green precipitate was observed. The reaction mixture was stirred at room temperature for 24 hrs. The desired product was recovered by filtration in vacuum, washed with water, diethyl ether and dried. 1.1302 g (Yield 69 %). Elemental analysis % for $C_{48}H_{55}ClCuN_4O_8$ was expected C 63.01, H 6.06, N 6.12, found C 63.12, H 6.11, N 6.09. ESI-MS. *m/z* found (calc.): 814.2 (814.3) for $[Cu(phen)_2(UDCA\text{-}H)]^+$, with the expected isotopic pattern. FT-IR (KBr), cm^{-1}:1565 $\upsilon_{asym}(OCO)$, 1375 $\upsilon_{sym}(OCO)$.

Determination of the reducing activity by DPPH method

Test compounds were dissolved in DMSO at 1.0 mM concentration, then a 1:10 dilution was performed with absolute ethanol. Stock solutions of DPPH (0.1 mM, absolute ethanol) were stored in the dark and used in a few hours. 1500 µL of the test solutions were directly added in a cuvette having an equal volume of DPPH, and the absorbance (200 - 650 nm range) was

recorded for 70 minutes at 25 °C. The absorbance at 517 nm was evaluated to examine the time-dependence of the radical scavenging activity (RA).[35,36]

Soybean lipoxygenase inhibition study

Stock solutions of C0, UDCA and C0-UDCA were dissolved in DMSO at ≈ 0.1 mM concentration, then the proper dilution was performed with TRIS buffer at pH 7.4. Sodium linoleate (0.00200 g, V 10.0 mL, ≈ 0.65 mM) and soybean lipoxygenase (0.00200 g, V 10.0 mL, ≈ $2 \cdot 10^{-6}$ M) were dissolved in TRIS buffer at pH 7.4, then the required dilutions were performed with TRIS buffer at pH 7.4. Solutions of sodium linoleate, soybean lipoxygenase and UDCA or C0-UDCA were prepared daily and kept in the dark at 5°C. The conversion of sodium linoleate to 13-hydroperoxylinoleic acid was monitored recording the absorbance at 243 nm and compared with the appropriate standard inhibitor caffeic acid. The absorbance at 243 nm and not at 234 nm (maximum) was chosen since at 234 nm the contribution of C0 or C0-UDCA absorbance was not negligible.

DFT calculations

Geometry optimization of deprotonated UDCA (UDCA-H) and $[Cu(phen)_2(UDCA\text{-}H)]^+$ were performed on an Intel-i7 based system using the release 4.2.0 of ORCA.[37] Input files for DFT calculations were prepared using Avogadro 1.2.0.[38] Geometry optimizations were performed at DFT level, using the hybrid PBE0 functional[39] and def-2 TZVP basis set.[40] The choice of the computational setup has been made based on the results previously reported for similar Cu(II)-phenanthroline systems.[11] IR frequency calculations were carried out to verify the nature of the minima of each optimization by assessing the absence of calculated negative frequencies. Atomic charges at natural population analysis (NPA) level were calculated by means of JANPA software package.[41] Molecular orbital shapes and energies were investigated using Chemcraft v1.8.[42]

Molecular Docking

Molecular docking calculations were performed using Autodock Vina software.[43] DFT-optimized structure of UDCA-H and C0-UDCA were exported as PDB files. The X-ray structure of the complex between soybean lipoxygenase and 3,4-dihydroxybenzoic acid (PDB:1N8Q) was chosen as the receptor. Prior to docking, both ligands and receptor were processed using MG Labs Autodock Tools.[44] In the receptor structure, both 3,4-dihydroxybenzoic acid (dhb) and water molecules were removed, while polar hydrogens and Gasteiger charges were added. The atomic charge for the Fe2840 cofactor was manually adjusted in the generated pdbqt file. For all the ligands, polar hydrogens and Gasteiger charges were added, while no rotational constraints were applied. Atomic charges for copper were manually adjusted in the generated pdbqt files. Validation of the docking protocol have been previously performed.[11]

The ligands were docked using a grid cube of 20 × 20 × 20 points centred at Iron cofactor coordinates (x = 21.287, y = 1.743, z = 19.171), or using a grid cube of 30 × 25 × 20 points at coordinates x = 24.970, y = 11.444, z = -0.396. A spacing of 1.0 Å and an exhaustiveness value of 100 was chosen in both cases. Molecular interactions and docked poses were evaluated using Biovia Discovery Studio Viewer 2021 (Dassault Systèmes, San Diego, CA, USA).

Intact Cell MALDI-TOF MS: Sample preparation

Intact Cell (IC) MALDI sample preparation was described in our publications previously reported [4546]. Briefly, matrix solution was prepared by dissolving 30 mg of Sinapinic Acid (SA) in 1 mL of CH_3CN/H_2O/Trifluoroacetic Acid (TFA) = 70/30 obtaining 7.5% of TFA. Frozen cell pellets were thawed on ice and diluted with cold Avidin-Biotin Complex (ABC).The cell suspensions were mixed

with SA matrix to reach ~25 000 cells per spot. Then, 2 µL of the resulting mixture were spotted on 384-well ground steel target on n technical replicates (n = 5) and dried at lab conditions.

Intact Cell MALDI-TOF MS: Spectra acquisition

IC MALDI-TOF MS of cell populations was performed on MALDI 7090 TOF-TOF instrument equipped with 2 kHz ultra-fast solid-state UV laser (Nd-YAG: 355 nm) and variable beam focus from 10 µm to >100 µm (Shimadzu Kratos Analytical). Mass spectra were acquired in the linear positive ion mode, in mass region 2 – 20 kDa, pulse extraction was set to 12,5 kDa and calibration was performed externally using the Bacterial Test Standard 3.5 – 17 kDa (Bruker Daltonics).

Biological assay

Cell culture conditions

Ovarian cancer cell line SKOV-3 was obtained from the American Type Culture Collection (ATTC), pancreatic cell line PANC-1 was obtained as a gift from collaborating laboratory of dr. Souček. Prior to use, the cell lines were authenticated via short tandem repeat (STR) profiling, which confirmed the cell identity. Mycoplasma contamination was investigated on a routine basis using PCR. All cell lines were cultured in high glucose (4.5 g L^{-1}) Dulbecco's Modified Eagle

Medium (DMEM) enriched with 10% fetal calf serum (FCS) (Invitrogen, Life Technologies, Czech Republic), 50 U/mL penicillin G, and 50 mg/mL streptomycin sulphate (PAA, GE Healthcare, Austria) at 37 °C in a humidified atmosphere with 5% CO_2. To specifically induce ER-stress by disruption of N-glycosylation, 1 mg/mL tunicamycin stock solution in DMSO (Sigma Aldrich, Czech Republic) was used at the indicated concentrations. ER-stress signaling was modulated by TUDCA (tauroursodeoxycholic acid, 2-[[(4R)-4-[(3R,5S,7S,8R,9S,10S,13R,14S,17R)-3,7-dihydroxy-10,13-dimethyl-2,3,4,5,6,7,8,9,11,12,14,15,16,17-tetradecahydro-1H-cyclopenta[a]phenanthren-17-yl]pentanoyl]amino]ethanesulfonic acid) dissolved in water to make 100 mg ml^{-1} stock solution (Sigma Aldrich, Czech Republic) and used at the indicated concentrations.

Cell viability assay

Cells were cultured for 24 h on a 96-well plate at a density of 10 000 cells per well in medium containing C0, TUDCA or C0-UDCA at the indicated concentrations. DMSO was used as a control. Then, the MTT reagent (3- (4,5-dimethylthiazol-2-yl)-2,5-diphenyltetrazolium bromide) (Sigma-Aldrich, Czech Republic) was added directly to the culture medium for 4 h. Then, the medium including MTT reagent was aspirated, and the cells lysed by addition of 90% isopropanol, 0.04 M HCl and 10% Triton/Tween. Absorbance was recorded at 570 nm by a Synergy HTX multi-mode reader (BioTek Instruments, VT, USA). All measurements were performed in technical pentaplicates and repeated in three independent biological experiments.

Cell growth assay

Cells were cultured for 24-72 h on a 6-well plate at a density of 20 000 cells per well in medium containing C0, TUDCA or C0-UDCA at the indicated concentrations. DMSO was used as a control. Cells were enzymatically detached, washed in Phosphate Buffer Saline (PBS) and counted using a Bürker counting chamber. Growth experiments were repeated in three independent biological experiments.

Immunoflurescence staining

Cells were cultured in 1.5 H microscopic glasses, treated with compounds for 24 hours and then fixed using 4% formaldehyde. Cells were washed twice with PBS and for immunofluorescent staining washed with 1x PBS containing 3% BSA and 0.1% Triton X-100 and incubated with DDIT3 (#2895), GRP-78 (#3177) or ATF6 (#65880)

antibodies (Cell Signaling, MA, USA) of phalloidin, diluted 1:500 at room temperature for 2 hours. Immunofluorescent signals were obtained by Alexa Fluor conjugated secondary antibodies (AF488, cat. no. A32731 or AF568, cat. no. A11004, both from Life Technologies, USA), diluted 1:2000. Cell nuclei were visualized by a Hoechst dye (Life Technologies, USA). Cells were then mounted and scanned by the inverted microscope Zeiss Axio Imager.

Flow cytometry

Vital staining of apoptotic cells was performed using FITC-conjugated annexin V (Roche Diagnostics, Mannheim, Germany) and propidium iodide. The cells were washed twice with staining buffer (10 mM HEPES, 140 mM NaCl, 10 mM $CaCl_2$, pH 7.4), incubated with annexin V-FITC (0.5 ll/sample) and propidium iodide (5 lg ml^{-1}) for 15 min and analysed by flow cytometry (BD FACS Aria^{TM} II Cell Sorter). At least 10 000 viable cells were collected for each sample. Flow cytometric data were analyzed using FlowJoTM 7.2.2. software (Becton–Dickinson). Results were evaluated as a percentage of double-negative cells (intact), annexin V-positive cells (early apoptotic), and double-positive (necrotic or late apoptotic) cells.

SDS-PAGE and western blotting

Trypsinised cells were washed two times with ice-cold PBS and resuspended in SDS lysis buffer (100 mM TRIS-HCl, 1% SDS, and 10% glycerol). Protein content in the cell extract was quantified using the Bradford-based BioRad protein Assay Kit (BioRad). Cell extracts were mixed with Laemmli sample buffer (100 mM Tris pH 6.8, 4% SDS, 200 mM DTT, 20% glycerol, and 0.1% bromophenol blue) and boiled for 3 min. An equivalent of 10 µg proteins was resolved using 10% sodium dodecyl sulphate polyacrylamide gel electrophoresis (SDS-PAGE). Resolved proteins were then electroblotted onto a 0.45 mm polyvinylidene difluoride (PVDF) membrane (Millipore, USA) and incubated with the indicated primary antibodies diluted 1:200 – 1:1000 at 4°C overnight (Actin cat. no: Ab1801, from Abcam, UK; DDIT3 #2895, and GRP-78 #3177; from Cell Signaling, MA, USA). Blots were developed using horseradish peroxidase (HRP)-conjugated anti-rabbit HRP #7074 or anti-mouse HRP #7076 (both Cell Signaling, USA) secondary antibodies, diluted 1:7500, and Immobilon Western HRP Substrate (Millipore, USA), according to the manufacturer's protocols.

Acknowledgments

S. M. thank MIUR for his PhD fellowship (XXXIV cycle). F. M. thank MIUR for her PhD fellowship (XXXVIII cycle). The authors thank the CeSAR (Centro Servizi Ricerca d'Ateneo) core facility of the University of Cagliari for the High-Resolution Mass Spectrometry experiments performed with Orbitrap Elite, Thermo Fisher Scientific, and to Masaryk University (MUNI/A/1301/2022). L.M. is supported by funds from the Faculty of Medicine MU to junior researcher (Lukáš Moráň, ROZV/28/LF/2020), supported by MH CZ-DRO (Masaryk Memorial Cancer Institute, 00209805) and Brno PhD Talent scholarship holder, funded by the Brno City Municipality.

References

1 J.-F. Goossens and C. Bailly, *Pharmacol Ther*, 2019, **203**, 107396.

2 L. Dyakova, D. C. Culita, G. Marinescu, M. Alexandrov, R. Kalfin, L. Patron and R. Alexandrova, *Biotechnology and Biotechnological Equipment*, 2014, **28**, 543–551.

3 J. Chung, S. H. An, S. W. Kang and K. Kwon, *PLoS One*, 2016, **11**, 1–18.

4 U. Beuers, J. L. Boyer and G. Paumgartner, *Hepatology*, 1998, **28**, 1449–1453.

5 J.-F. Goossens and C. Bailly, *Pharmacol Ther*, 2019, **203**, 107396.

6 A. L. Cao, L. Wang, X. Chen, Y. M. Wang, H. J. Guo, S. Chu, C. Liu, X. M. Zhang and W. Peng, *Laboratory Investigation*, 2016, **96**, 610–622.

7 F. Trudu, F. Amato, P. Vaňhara, T. Pivetta, E. M. Peña-Méndez and J. Havel, *J Appl Biomed*, 2015, **13**, 79–103.

8 C. Santini, M. Pellei, V. Gandin, M. Porchia, F. Tisato and C. Marzano, *Chem Rev*, 2014, **114**, 815–862.

9 S. Masuri, P. Vaňhara, M. G. Cabiddu, L. Moráň, J. Havel, E. Cadoni and T. Pivetta, *Molecules*, 2022, **27**, 49.

10 L. Moráň, T. Pivetta, S. Masuri, K. Vašíčková, F. Walter, J. Prehn, M. Elkalaf, J. Trnka, J. Havel and P. Vaňhara, *Metallomics*, 2019, **11**, 1481–1489.

11 S. Masuri, E. Cadoni, M. G. Cabiddu, F. Isaia, M. G. Demuru, L. Moráň, D. Buček, P. Vaňhara, J. Havel and T. Pivetta, *Metallomics*, 2020, **12**, 891–901.

12 R. Sano and J. C. Reed, *Biochim Biophys Acta Mol Cell Res*, 2013, 1833, 3460–3470.

13 S. Munshi and R. Dahl, *Bioorg Med Chem*, 2016, **24**, 2382–2388.

14 U. Ozcan, E. Yilma, L. Özcan, M. Furuhashi, E. Vaillancourt, R. O. Smith, C. Z. Görgün and G. S. Hotamisligil, *Science (1979)*, 2006, **313**, 1137–1140.

15 P. Vaňhara, L. Moráň, L. Pečinka, V. Porokh, T. Pivetta, S. Masuri, E. Maria Peña-Méndez, J. Elías Conde González, A. Hampl and J. Havel, in *Mass Spectrometry in Life Sciences and Clinical Laboratory*, IntechOpen, 2021.

16 P. Vaňhara, L. Kučera, L. Prokeš, L. Jurečková, E. M. Peña-Méndez, J. Havel and A. Hampl, *Stem Cells Transl Med*, 2018, **7**, 109–114.

17 C. Hao and R. E. March, *Journal of Mass Spectrometry*, 2001, **36**, 509–521.

18 J. P., *Ann. Chim. Appl.*, 1928, **9**, 113–203.

19 J. S. Renny, L. L. Tomasevich, E. H. Tallmadge and D. B. Collum, *Angewandte Chemie International Edition*, 2013, **52**, 11998–12013.

20 T. Pivetta, M. D. Cannas, F. Demartin, C. Castellano, S. Vascellari, G. Verani and F. Isaia, *J Inorg Biochem*, 2011, **105**, 329–338.

21 G. Deacon and R. J. Phillips, *Coord Chem Rev*, 1980, **33**, 227–250.

22 K. Nakamoto, *Infrared and Raman Spectra of Inorganic and Coordination Compounds*, John Wiley & Sons, Inc., Hoboken, NJ, USA, 2008.

23 A. W. Addison, T. N. Rao, J. Reedijk, J. van Rijn and G. C. Verschoor, *J. Chem. Soc., Dalton Trans.*, 1984, 1349–1356.

24 M. Devereux, M. McCann, J. F. Cronin, G. Ferguson and V. McKee, *Polyhedron*, 1999, **18**, 2141–2148.

25 F. Clifford, E. Counihan, W. Fitzgerald, K. Seff, C. Simmons, S. Tyagi and B. Hathaway, *J Chem Soc Chem Commun*, 1982, 196.

26 M. Barceló-Oliver, Á. García-Raso, Á. Terrón, E. Molins, M. J. Prieto, V. Moreno, J. Martínez, V. Lladó, I. López, A. Gutiérrez and P. V. Escribá, *J Inorg Biochem*, 2007, **101**, 649–659.

27 K. N. Lazarou, S. P. Perlepes, V. Psycharis and C. P. Raptopoulou, *Polyhedron*, 2008, **27**, 2131–2142.

28 A. R. Brash, *Journal of Biological Chemistry*, 1999, **274**, 23679–23682.

29 R. Wisastra and F. Dekker, *Cancers (Basel)*, 2014, **6**, 1500–1521.

30 F. Isaia, M. C. Aragoni, M. Arca, C. Caltagirone, C. Castellano, G. de Filippo, A.

Garau, V. Lippolis and T. Pivetta, *Green Chemistry*, 2017, **19**, 4591–4599.

31 M. Strohalm, D. Kavan, P. Nova and M. Volny, *Anal Chem*, 2010, **82**, 4648–4651.

32 T. H. J. Niedermeyer and M. Strohalm, *PLoS One*, 2012, **7**, e44913.

33 P. Gans, A. Sabatini and A. Vacca, *Talanta*, 1996, **43**, 1739–1753.

34 J. P., *Ann. Chim. Appl.*, 1928, **9**, 113–203.

35 C. Tolia, A. N. Papadopoulos, C. P. Raptopoulou, V. Psycharis, C. Garino, L. Salassa and G. Psomas, *J Inorg Biochem*, 2013, **123**, 53–65.

36 Z. Boulsourani, G. D. Geromichalos, S. Katsamakas, V. Psycharis and C. P. Raptopoulou, *Materials Science & Engineering C*, 2019, **94**, 493–508.

37 F. Neese, *Wiley Interdiscip Rev Comput Mol Sci*, 2012, **2**, 73–78.

38 M. D. Hanwell, D. E. Curtis, D. C. Lonie, T. Vandermeersch, E. Zurek and G. R. Hutchison, *J Cheminform*, 2012, **4**, 17.

39 C. Adamo and V. Barone, *Journal of Chemical Physics*, 1999, **110**, 6158–6170.

40 F. Weigend and R. Ahlrichs, *Physical Chemistry Chemical Physics*, 2005, **7**, 3297–3305.

41 T. Y. Nikolaienko, L. A. Bulavin and D. M. Hovorun, *Comput Theor Chem*, 2014, **1050**, 15–22.

42 Chemcraft - graphical software for visualization of quantum chemistry computations. https://www.chemcraftprog.com.

43 O. Trott and A. J. Olson, *J Comput Chem*, 2009, 455–461.

44 G. M. Morris, H. Ruth, W. Lindstrom, M. F. Sanner, R. K. Belew, D. S. Goodsell and A. J. Olson, *J Comput Chem*, 2009, **30**, 2785–2791.

45 M. Deulofeu, L. Kolářová, V. Salvadó, E. María Peña-Méndez, M. Almáši, M. Štork, L. Pour, P. Boadas-Vaello, S. Ševčíková, J. Havel, J. Havel and P. Vaňhara, *Sci Rep*, , DOI:10.1038/s41598-019-44215-1.

46 E. Valletta, L. Kučera, L. Prokeš, F. Amato, T. Pivetta, A. Hampl, J. Havel and P. Vaňhara, *PLoS One*, , DOI:10.1371/journal.pone.0147414.